22 March 2002

Summary of ATRAP[+] Progress for the SPSC

G. Gabrielse[*], J. Estrada, J.N. Tan, P. Yesley, N.S. Bowden, P. Oxley,
C.H. Storry, M. Wessels, J. Tan
Department of Physics, Harvard University, Cambridge, MA 02138

D. Grzonka, W. Oelert, G. Schepers, T. Sefzick
IKP, Forschungszentrum Jülich GmbH, 52425 Jülich, Germany

J. Walz
CERN EP Division, 1211 Geneva 23, Switzerland

T.W. Hänsch
Max-Planck-Institut für Quantenoptik, Hans-Kopfermann-Strasse 1, 85748 Garching, Germany

E. Hessels
Department of Physics, York University, 4700 Keele St., Toronto, Canada M3J1P3

H. Kalinowsky
Institut für Strahlen-und Kernphysik, University of Bonn, 53115 Bonn, Germany

[+] Antihydrogen Trap Collaboration, http://hussle.harvard.edu/~atrap.
[*] Spokesperson, gabrielse@physics.harvard.edu.

Published Sections of This Summary

During the months of 2001 that antiprotons were available at the AD, ATRAP was able to investigate the interaction of cold antiprotons and cold positrons – a unique capability of ATRAP so far. A discussion of the techniques used to accomplish this interaction is in a section of this report that was published during 2001 in

"First Positron Cooling of Antiprotons"
G. Gabrielse, J. Estrada, J.T. Tan, P. Yesley, N.S. Bowden, P. Oxley, T. Roach, C.H. Storry, M. Wessels, J. Tan, D. Grzonka, W. Oelert, G. Schepers, T. Sefzick, W.H. Breunlich, M. Cargnelli, H. Fuhrmann, R. King, R. Ursin, J. Zmeskal, H. Kalinowsky, C. Wesdorp, J. Walz, K.S.E. Eikema, T.W. Hänsch
Physics Letters B 507, 1-6 (2001).

Another section of this report was also published during 2001. It contains an encouraging theoretical investigation of the possibility to simultaneously confine cold neutral antihydrogen, along with the cold charged ingredients from which it is formed.

"Stability of a Charged Particle in a Combined Penning-Ioffe Trap"
T.M. Squires, P. Yesley, and G. Gabrielse
Physical Review Letters 86, 5266-5269 (2001).

While more theoretical work is needed, and experimental investigations are crucial, the start is very encouraging.

Experimental Progress Itemized

Experimental advances during 2001 include the following. These were carefully described and illustrated in the oral presentation to the SPSC. Extensive calculation and simulation is underway to allow us to better understand what was observed. When this analysis is completed a substantial paper will be submitted for publication.

1. Robust techniques to simultaneously accumulate cold antiprotons and cold positrons were developed and demonstrated. The SPSC was shown "movies" of the intricate particle manipulations that are involved.

2. Positron cooling of antiprotons was carefully studied because it offers a way to produce positrons and antiprotons with a low relative velocity – conditions under which cold antihydrogen is expected to form. Cooling time constants were measured and the energy spectra of the antiprotons were measured as a function of cooling time.

3. Techniques to allow launching, reflection and recapturing cold positron and antiproton bunches from location in our trap structure to another region of our trap structure were developed and demonstrated. These techniques will allow us to investigate the pulsed field recombination technique, to eliminate impurities particles from our traps, and to set the initial conditions for the investigation of other recombination methods.

4. Electron-cooling, magnetron-cooling, resistor-cooling, and sideband-cooling are just some of the names describing processes that are required (in addition to positron cooling) to make the cold plasmas from which cold antihydrogen will form robustly. We spent a lot of time studying these processes, and combinations of these processes, since only with cold antihydrogen is there hope to make precise measurements.

5. We carefully studied the spatial distribution and the density of trapped antiprotons and trapped positrons, as a function of the number of trapped particles. Good control of these parameters is crucial for achieving the robust production of cold antihydrogen.

6. We observed intriguing signals that suggested the possible formation of cold antihydrogen atoms. At the time of the oral report to the SPSC we were not yet confident that an alternate explanation could be eliminated. There is a lot of theoretical effort being focused upon a better understanding of our intriguing signals, and a theory workshop being held soon will have this as a central topic. Although some elaboration follows, definite conclusions must wait until our analysis is completed.

Analysis Continues on Promising Signals

By manipulating the electric trapping fields, ATRAP was able to nudge cold positrons and antiprotons together using a carefully controlled time sequence. We next applied a "clearing field" to clear any free antiprotons and positrons from the interaction region. This field would also ionize the less strongly bound of any Rydberg antihydrogen atoms that may have been formed. Antihydrogen atoms that are not ionized, being neutral, would not be accelerated from the interaction region by the clearing field. We next applied a stronger ionizing electric field in such a way that any Rydberg antihydrogen atoms that remained in the interaction region would be ionized and their antiprotons would be captured. We can detect such captured antiprotons with unit efficiency.

We see no such signals if positrons are not present, and we do see such signals when positrons are present. The signal we see also declines as we increase the strength of the clearing field, consistent with our expectation that this clearing field would not only clear charged particles from the interaction region, it would also field ionize the higher Rydberg states. The signals we see are thus consistent with the production of cold antihydrogen atoms.

The alternate explanation, discussed in the oral report to the SPSC, was that we produced a nearly neutral, ultra cold plasmas of antiprotons and positrons. More analysis has cast some doubt on this alternate explanation, but it is still under very active theoretical investigation. Calculations, simulations, and modeling underway should allow a better understanding of what is taking place. Until these studies are completed we are being very cautious about what we say to discourage any unwarranted publicity. (Our cautious approach did not keep a reporter from the New Scientist from broadcasting misunderstandings of a scientific presentation in a conference.)

2002

During 2002, we will study the intriguing signals we have observed with better controlled timing and diagnostics. The basic idea is to look for a unique time signature that can only be produced by the formation of Rydberg antihydrogen. What will differ from last year is that we will have much better control of the electric fields used to nudge fields together, to clear charged particles, and to ionize any antihydrogen that is formed. We will be able to vary the timing of the various crucial parts of this cycle. We will also investigate several variants of the way that antiprotons and positrons are made to interact.

In addition, a second apparatus under construction should be completed and put into operation in 2002. It will allow us to also explore a laser assisted recombination mechanism and a cesium charge exchange recombination mechanism. This apparatus is constructed so that it can be inserted as a replacement for the existing trap apparatus during a weekend.

Not surprisingly, a hope of the medium and high energy experimenters in the committee is that traditional particle detection could identify antihydrogen, by detecting a simultaneous annihilation of a positron and an antiproton when an antihydrogen atom hits a solid surface. This unfortunately is not possible because of false positron events generated from antiproton annihilation on a nucleus. The best that can be hoped for are antiproton annihilation events that have an increased probability of accompanying positron events when positrons are present. We will attempt this. However, it is also important to recall that the objective of the antihydrogen experiments is not to identify the production of a small number of antihydrogen atoms. The goal is the robust production of enough cold antihydrogen atoms to allow precise spectroscopic comparisons of antihydrogen and hydrogen.

We wish that the number of weeks that antiprotons are available during 2002 was being increased rather than decreased, since one frustration is that the data rate is very slow at the AD. We can only make an attempt or two per hour to make cold antihydrogen, and we typically have only an eight hour shift each week day. (It has been agreed to develop and implement a method of switching antiprotons between experiments each hour to allow making more efficient use of the AD antiprotons. This will help.) Despite the challenge, we are confident that progress will continue during 2002

ATRAP-2

The experiments we are carrying out right now we call ATRAP-1. These experiments are done in a prototype trap apparatus whose 4.2 K diameter is about 10 cm.

We have expended a huge effort in recent years to design, and construct the ATRAP-2 apparatus that has a much larger diameter. Delays in the delivery of the large superconducting solenoid have slowed our progress here, but a lot of apparatus has been constructed. Installation into our second beam zone has begun and will continue throughout the year. Installation and testing of the new apparatus should not hamper the prototype, ATRAP-1 experiments that will continue at the first of the two ATRAP antiproton access ports.

17 May 2001

PHYSICS LETTERS B

ELSEVIER

Physics Letters B 507 (2001) 1–6

www.elsevier.nl/locate/npe

First positron cooling of antiprotons

G. Gabrielse [a], J. Estrada [a], J.N. Tan [a], P. Yesley [a], N.S. Bowden [a], P. Oxley [a], T. Roach [a,1], C.H. Storry [a], M. Wessels [a], J. Tan [a], D. Grzonka [b], W. Oelert [b], G. Schepers [b], T. Sefzick [b], W.H. Breunlich [c], M. Cargnelli [c], H. Fuhrmann [c], R. King [c], R. Ursin [c], J. Zmeskal [c], H. Kalinowsky [d], C. Wesdorp [e], J. Walz [f,2], K.S.E. Eikema [f], T.W. Hänsch [f]

[a] *Department of Physics, Harvard University, Cambridge, MA 02138, USA*
[b] *IKP, Forschungszentrum Jülich GmbH, 52425 Jülich, Germany*
[c] *Institute for Medium Energy Physics, Boltzmanngasse 3, 1090 Vienna, Austria*
[d] *Institut für Strahlen-und Kernphysik, University of Bonn, 53115 Bonn, Germany*
[e] *FOM Institute for Atomic and Molecular Physics, Kruislaan 407, 1098 SJ, 1098 SJ, Amsterdam, Netherlands*
[f] *Max-Planck-Institut für Quantenoptik, Hans-Kopfermann-Strasse 1, 85748 Garching, Germany*

Received 28 March 2001; accepted 3 April 2001
Editor: L. Montanet

Abstract

Positrons are used to cool antiprotons for the first time. The oppositely charged positrons and antiprotons are first simultaneously accumulated in separate Penning trap volumes, and then are spatially merged in a nested Penning trap. The antiprotons cool until they reach a low relative velocity with respect to the cold positrons, the situation expected to be optimal for the production of cold antihydrogen. © 2001 Published by Elsevier Science B.V.

Simultaneous electrical signals from separated positrons and antiprotons, first at CERN [1] then at Fermilab [2], confirmed the fleeting existence of several antihydrogen atoms, the first observed atoms made entirely of antimatter. The small number and brief existence of these bound states of positrons and antiprotons, traveling at nearly the speed of light, make any comparison of the properties of antihydrogen and hydrogen at an interesting level of accuracy to be extremely unlikely.

Cold antihydrogen atoms (at temperatures not far from absolute zero) have not yet been observed, but offer the exciting prospect of antihydrogen captured in a magnetic trap [3] long enough to use lasers to probe for any difference between antihydrogen and hydrogen. The ingredients of cold antihydrogen have been previously confined in the same trap structure [4]. This letter from the ATRAP Collaboration [5] reports the first observation of positron cooling of antiprotons, the closest approach yet to the production of cold antihydrogen. The antiprotons cool to a low relative velocity with respect to the positrons, a condition expected to facilitate the production of cold antihydrogen.

The antiprotons come from CERN's new Antiproton Decelerator (AD) [6]. Late in 2000 the AD started delivering 330 ns pulses of 5 MeV antiprotons, with

E-mail address: gabrielse@physics.harvard.edu (G. Gabrielse).

[1] New address: College of the Holy Cross, Worcester, MA 01610, USA.

[2] New address: CERN, 1211 Geneva 23, Switzerland.

0370-2693/01/$ – see front matter
PII: S0370-2693(01)00450-6

3×10^7 antiprotons per pulse in the best case. This is a hundred times fewer antiprotons per pulse than was available from the three-storage-ring complex (ACOL, AA and LEAR) that the AD replaced. However, pulses are sent much more often — every 110 seconds — and can be accumulated more inexpensively in a trap [7] than in a complex involving several storage rings.

The 5 MeV antiprotons from the AD are accumulated at 4.2 K, an energy reduction greater than 10^{10}. The required techniques to slow, trap, cool, and accumulate these antiprotons [7–10] were recently reviewed [11]. They were developed by the TRAP Collaboration, the predecessor of ATRAP. Positrons from a 110 mCi ^{22}Na source are also slowed, trapped, cooled and accumulated at 4.2 K. High Rydberg positronium is formed, and then ionized and captured at a rate that exceeds the recent first demonstration of this technique [12] by a factor of 27.

The intricate trap apparatus (Fig. 1) within which the antiprotons and positrons are captured, cooled and accumulated includes 32 ring electrodes stacked vertically. A 6 Tesla magnetic field (from a superconducting solenoid) is parallel to the central symmetry axis of the trap electrodes. Each of these electrodes is made of gold-plated OFE copper with a 1.2 cm inner diameter. Appropriate potentials on any three (or five) adjacent electrodes form a Penning trap for charged particles [13]. The electrodes are within a copper vacuum enclosure sealed with indium and cooled to 4.2 K via a thermal contact to liquid helium. The long (> 3.2 months) lifetime of trapped antiprotons within a similar container established a pressure less than 5×10^{-17} Torr [10]. (No magnetic trap for antihydrogen was used in this first demonstration.)

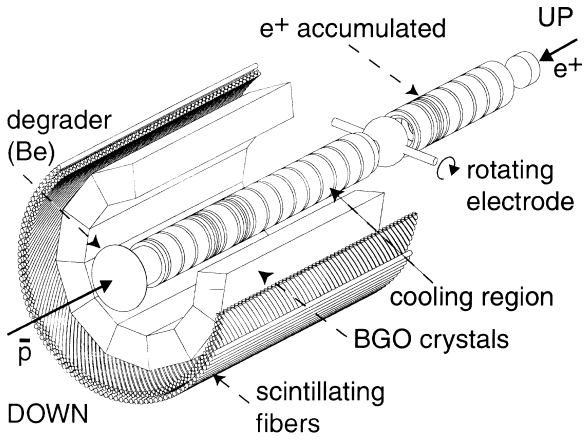

Fig. 1. Overview of the trap and detectors.

A rotatable electrode separates an upper region (where positrons are trapped and accumulated) from a lower region (where antiprotons are trapped and accumulated at the same time). This unusual electrode can be rotated while at low temperature, while within the extremely high vacuum, and in the presence of a high field. The 6 Tesla field, and a current sent through coils attached to the electrode, generate the required torque. In its closed position this electrode prevents antiprotons from disrupting the positron loading, as observed earlier [4,12]. After the accumulations, the electrode is rotated to its open position to allow trapped positrons to join the antiprotons.

The trap is surrounded by layers of detectors (Fig. 1) that are just outside a thin copper vacuum enclosure (not shown in the figure). The BGO crystals, operated at 77 K, will be used later to detect photons from positron annihilation. Three layers of scintillating fibers, also near 77 K, detect charged pions from antiproton annihilation. The two inner layers are 1.5 mm diameter fibers in about 38.5 degree helices, offset to close the gaps between fibers. The 1.9 mm diameter fibers in the outer layer are vertical, and parallel to the axis of the trap. The superconducting solenoid that produces the vertical magnetic field, and its dewars, surround the scintillating fibers. A double layer of segmented plastic scintillators, surrounding the dewar, also detects pions from antiproton annihilation.

A coincidence of two of the three scintillating fiber layers detects an antiproton annihilation within the trap region with essentially 100% efficiency, but with a background counting rate of 55/s. A coincidence of the two outer scintillators detects an antiproton annihilation within the trap region with an efficiency of 50% but with a background counting rate of 75/s. A coincidence of both signals reduces the background counting rate to 3/s.

The pulsed antiproton beam from the AD is directed upward into our apparatus, where the antiprotons are centered within approximately a 4 mm diameter using a parallel plate avalanche detector operated in ionization mode. The energy of these antiprotons is varied slightly by changing the amount of SF_6 mixed with He in a 1.5 cm long gas cell, to maximize the

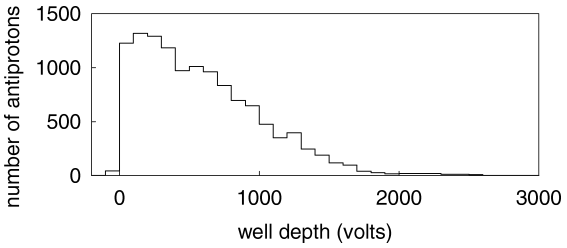

Fig. 2. Energy spectra for 12000 of the first antiprotons trapped from a single pulse of antiprotons from the AD.

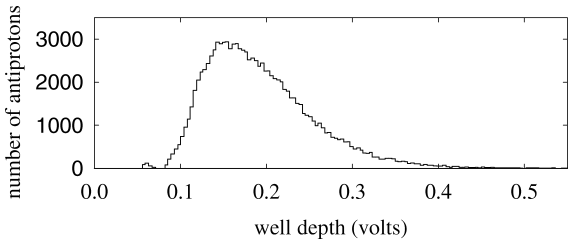

Fig. 3. Energy spectrum for 106000 of the first antiprotons electron-cooled and stacked at the AD.

number slowed below 4 keV in the 125 μm thick berylium degrader that follows the cell [9]. These slowed antiprotons are reflected by a -4 kV potential applied to an electrode just before the rotatable one. Before they can return to the degrader, its potential is pulsed to -4 kV to capture the antiprotons [8].

Up to 12000 antiprotons are captured in this 4 kV trap from a single pulse of antiprotons from the AD, an efficiency of about 5×10^{-4}, consistent with earlier measurements in a similar trap [11]. The energy of the trapped antiprotons is analyzed by slowly reducing the depth of the potential well that confines them (Fig. 2), and counting the annihilations of antiprotons that leave the trap. Because the energy spread of antiprotons emerging from the degrader is very wide compared to the energies we can capture, the number of trapped particles increases approximately linearly with the depth of the trapping well. A linear extrapolation suggests that in a larger trap with 20 kV potentials we could capture up to 40000 antiprotons per pulse.

We precool the antiprotons (before they interact with the separately accumulated positrons) by colliding them with 4.2 K electrons [7], the only stable matter species that can collide with antiprotons without annihilating them. The electrons are preloaded into several small wells within the trap before the antiprotons arrive. The electrons themselves cool rapidly via the spontaneous emission of synchrotron radiation until they reach equilibrium with the surrounding electrodes at 4.2 K. The captured antiprotons cool in tens of seconds as they travel back and forth through the electrons, transferring their energy to the cold electrons with which they collide. Up to 100% of the trapped antiprotons cool into the wells occupied by the cold electrons.

Once the antiprotons reside in the small wells with the cooling electrons we can inject and cool more pulses of antiprotons, using the same cooling electrons. Our automated apparatus routinely stacks more than 10^5 antiprotons (Fig. 3) while unattended. We have yet to investigate the accumulation of more antiprotons, but it should be possible since we are far from the space charge and Brillouin limits.

When we have stacked the desired number of antiprotons we slowly change the potentials on the trap electrodes to transfer all the antiprotons and electrons into one potential well within one electrode. Switching this potential well off for 300 ns then ejects the electrons, while the more massive antiprotons do not accelerate sufficiently to leave the trap.

Positrons accumulate in the upper trap region at the same time that antiprotons accumulate below. The new and efficient method for accumulating large numbers of 4.2 K positrons [12] is the only one yet demonstrated. Since these positrons accumulate directly in the highest field region, at 6 Tesla, we avoid the magnetic bounce that would reduce the number of positrons able to move from a weak to a strong magnetic field.

The positrons come from a 110 mCi ^{22}Na source that is 3 mm in diameter. This source is precooled to near 77 K and is lowered 2 m from its lead shielding enclosure, down through the helium dewar needed to keep the trap cold, until it settles against the 4.2 K trap enclosure. Positrons, whose energy distribution has a 0.5 MeV endpoint, follow magnetic field lines and enter the trap vacuum through a 10 μm thick Ti window. Some of them slow as they enter the trapping region through a 2 μm thick single crystal of tungsten. Others slow while turning around within a thick tungsten crystal that is rotated to the trap axis when the rotatable electrode is in its closed position. Neither crystal can be struck by antiprotons when the rotatable electrode is in its closed position. This leaves

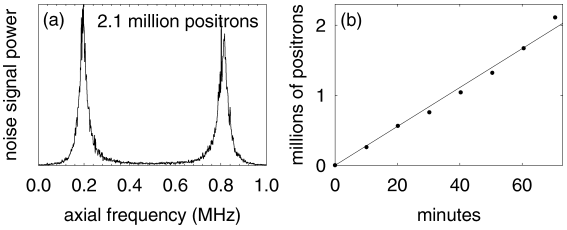

Fig. 4. (a) Electrical signal from 2.1 million trapped positrons. (b) Positrons accumulate at a rate 27 times higher than reported in a recent introduction to the technique.

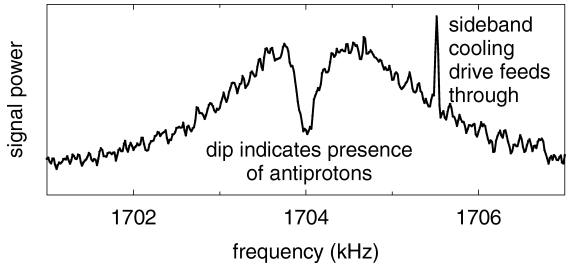

Fig. 5. Nondestructive electrical signal from trapped antiprotons which are cooled by the detector.

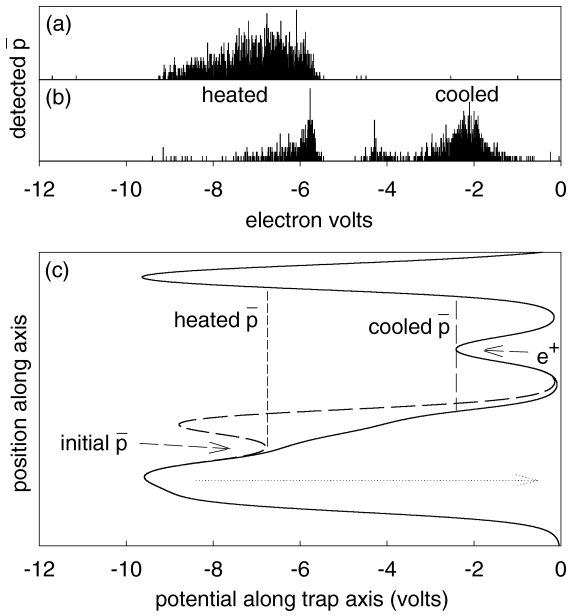

Fig. 6. (a) Uncooled antiproton spectrum. (b) Cooled antiproton spectrum shows some antiprotons are not cooled. (c) Potential wells for the positrons and antiprotons.

undisturbed the essential layer of absorbed gas on the thin crystal of tungsten, without which positron loading ceases [4,12].

Slow positrons that pick up electrons while leaving the thin crystal form Rydberg positronium atoms. These atoms travel parallel to the axis of the trap until they are ionized by the electric field of the trap well, and captured. The frequency spacing of the two peaks in the electrical signal induced across an RLC circuit attached to the trap reveals the number of accumulated positrons. Fig. 4(b) shows approximately 2 million positrons accumulating in an hour, a 27-fold increased rate compared to our recent report [12] announcing the method. Normalized to the source strength, the maximum rate we observe is 1.4×10^4 e^+ $\mathrm{h}^{-1}\,\mathrm{mCi}^{-1}$. This is a bit smaller than our previous rate, presumably because the larger source diameter compromises the positron accumulation. Switching the rotatable electrode to its open position allows positrons to be moved into the lower section of the trap with the antiprotons, with a transfer efficiency of 80% or higher.

Four radiofrequency detectors nondestructively detect the number of positrons (Fig. 4(a)) and other trapped particles, and damp oscillations of these particles. The particle motions induce detectable currents in resonant RLC circuits attached to trap electrodes, and the energy dissipated in these circuits is removed from the particle motions. Positron and electron motion along the magnetic field direction are so damped, as is similar antiproton (or proton) motion (Fig. 5), and antiproton (or proton) cyclotron motion. Positron and electron cyclotron motion damps via the spontaneous emission of synchrotron radiation, while magnetron drift motion of all particles can be reduced by sideband cooling [13].

Positron cooling of antiprotons is similar in principle to electron cooling of antiprotons. The motional energy of the trapped antiprotons is transferred to lighter trapped particles by Coulomb collisions, and the lighter particles cool rapidly via synchrotron radiation. There are two important differences in practice. First, since the positrons and antiprotons have an opposite sign of charge, they cannot be confined in the same Penning trap well. Our solution is the nested Penning trap [14] (Fig. 6(c)). The device and technique were investigated earlier with electrons and protons [15] though with far fewer electrons than the

number of positrons used here. The second difference is the obvious technical challenge of producing and manipulating two antimatter species, rather than two matter species.

A potential well containing cold antiprotons and electrons is adiabatically elevated as shown in Fig. 6(c). The antiprotons are launched into the nested trap, and given kinetic energy by pulsing the dashed potential curve to the solid curve. Simultaneously, the potential barrier at the opposite end of the nested well is pulsed near zero volts to encourage any electrons confined with the antiprotons to leave the well. Both barriers are restored to full height after 1.5 μs, before the slower antiprotons can make it from the launching point to the turning point. The antiprotons are now in a nearly symmetrical nested well structure.

Two minutes after the antiprotons are injected into the nested well, the energy distribution of the trapped antiprotons is analyzed by slowly lowering the potential barrier nearest the launch point (dotted arrow in Fig. 6(c)). When no positrons are present in the nested trap, Fig. 6(a) shows the number of annihilations of antiprotons released from the trap as a function of the remaining barrier height. In this example about 4000 antiprotons had kinetic energies distributed around 7 eV relative to the bottom of the potential well.

To demonstrate positron cooling we repeat this process but with approximately 250000 positrons preloaded into the inverted central well that is nested within the longer outer well. These positrons cool via synchrotron radiation to thermal equilibrium with their 4.2 K environment in only 0.1 seconds. They are collected into a volume that is a couple of millimeters in radius and length, with a density of 7×10^6 cm^{-3}. Antiprotons are launched into the nested trap exactly as before. The antiprotons that pass through the positron cloud are cooled by collisional transfer of energy to the positrons.

When we analyze the antiproton energy as before we see in Fig. 6(b) that most of the antiprotons have cooled to approximately the same level in the well that is occupied by the positrons. They do not cool below this energy because the cooling stops when the antiprotons have insufficient energy to reenter the positron cloud. There are also some antiprotons that are not cooled, presumably because they are located away from the center axis of the trap where there are no cold positrons. The number of uncooled antiprotons could likely be reduced by sideband cooling of the antiprotons before their launch. We do not yet understand the small intermediate energy peak of partially cooled antiprotons.

The cooled antiprotons have a low relative velocity with respect to the cold positrons that cooled them. A low relative velocity is one condition under which antihydrogen formation processes (e.g., radiative recombination and three body recombination) are expected to have their highest rates. These rates are nonetheless very small so that observing these processes will take much time and care. In addition, the electric fields of the trap will ionize any high Rydberg state produced by the latter process.

Much remains to be done before cold antihydrogen is observed and precise laser spectroscopy is performed. However, this first positron cooling of antiprotons demonstrates that it is possible to make the ingredients of cold antihydrogen interact at very low energies, and is the closest approach yet to cold antihydrogen.

Acknowledgements

We are grateful to CERN for constructing the new AD so that studies of cold antihydrogen could be carried out, to Japan, Germany, the United States, and Italy for the needed external support, and to the CERN PS Division and the AD team for making the AD deliver cooled antiprotons starting in July 2000. Since this is the first publication of the ATRAP Collaboration, we are especially grateful to our home institutions for the technical support and effort devoted to the construction of the ATRAP apparatus. This work was supported by the NSF, AFOSR, the ONR of the US, the German BMBF, the Austrian Academy of Sciences, and the FOM/NWO of The Netherlands.

References

[1] G. Baur et al., Phys. Lett. B 368 (1996) 251.
[2] G. Blanford et al., Phys. Rev. Lett. 80 (1998) 3037.
[3] G. Gabrielse, in: P. Bloch, P. Paulopoulos, R. Klapisch (Eds.), Fundamental Symmetries, Plenum, New York, 1987, p. 59.

[4] G. Gabrielse, D. Hall, T. Roach, P. Yesley, A. Khabbaz, J. Estrada, C. Heimann, H. Kalinowsky, Phys. Lett. B 455 (1999) 311.
[5] http://hussle.harvard.edu/~atrap.
[6] S. Maury, Hyperfine Int. 109 (1997) 43.
[7] G. Gabrielse, X. Fei, L. Orozco, R. Tjoelker, J. Haas, H. Kalinowsky, T. Trainor, W. Kells, Phys. Rev. Lett. 63 (1989) 1360.
[8] G. Gabrielse, X. Fei, K. Helmerson, S. Rolston, R. Tjoelker, T. Trainor, H. Kalinowsky, J. Haas, W. Kells, Phys. Rev. Lett. 57 (1986) 2504.
[9] G. Gabrielse, X. Fei, L. Orozco, S. Rolston, R. Tjoelker, T. Trainor, J. Haas, H. Kalinowsky, W. Kells, Phys. Rev. A 40 (1989) 481.
[10] G. Gabrielse, X. Fei, L. Orozco, R. Tjoelker, J. Haas, H. Kalinowsky, T. Trainor, W. Kells, Phys. Rev. Lett. 65 (1990) 1317.
[11] G. Gabrielse, Adv. At. Mol. Opt. Phys. 45 (2000) 1.
[12] J. Estrada, T. Roach, J. Tan, P. Yesley, D. Hall, G. Gabrielse, Phys. Rev. Lett. 84 (2000) 859.
[13] L.S. Brown, G. Gabrielse, Rev. Mod. Phys. 58 (1986) 233.
[14] G. Gabrielse, S. Rolston, L. Haarsma, W. Kells, Phys. Lett. A 129 (1988) 38.
[15] D. Hall, G. Gabrielse, Phys. Rev. Lett. 77 (1996) 1962.

Stability of a Charged Particle in a Combined Penning-Ioffe Trap

T. M. Squires, P. Yesley, and G. Gabrielse
Department of Physics, Harvard University, Cambridge, Massachusetts 02138
(Received 19 January 2001)

The axial symmetry of a familiar Penning trap is broken by adding the radial magnetic field of an Ioffe trap. Despite the resulting loss of a confinement theorem, stable orbits related to adiabatic invariants are identified, expressions are given for their frequencies, and resonances that must be avoided are characterized. It seems feasible to experimentally realize the new Penning-Ioffe trap to test these theoretical predictions. It also may be possible to simultaneously confine cold positrons and antiprotons in a Penning-Ioffe trap, along with any cold antihydrogen they may form.

DOI: 10.1103/PhysRevLett.86.5266 PACS numbers: 41.20.–q, 41.90.+e

The stability of charged particles in a Penning trap (a uniform magnetic field along the symmetry axis of an electrostatic quadrupole) makes it one of the versatile devices of modern physics. Classical and quantum descriptions are elegant and exact [1]. Individual elementary particles in a Penning trap are used to test QED, determine the fine structure constant, test *CPT* with leptons and baryons, and carry out accurate mass spectroscopy. Many electrons and ions stored in such traps allow measurements of the masses of unstable nuclei, ion cyclotron resonance analysis of pharmaceuticals and biological materials, and (often in closely related Malmberg traps [2]) permit studies of single component plasmas.

The stability is closely related to axial symmetry; the resulting conservation of angular momentum gives rise to a confinement theorem [3]. Neither one charged particle nor a dense single-component plasma can spread perpendicularly to the magnetic field and leave a Penning or Malmberg trap. In this Letter we investigate the breakdown of this symmetry and confinement theorem. We add the radial magnetic quadrupole field of an Ioffe trap — an experimentally realizable modification, characterized by only one parameter. (An alternative is distorting the electrostatics of the trap [4].) A Ioffe trap is a familiar way to confine neutral particles [5]. An intriguing question is whether a Penning-Ioffe trap (e.g., Fig. 1a) could confine cold antihydrogen atoms along with the charged antiprotons ($\bar{p}$) and positrons (e^+) from which they form. The stability of the charges is crucial; they must remain confined long enough for neutral atoms to form.

The Penning-Ioffe system and the analysis of the motion of a charged particle within it are simple and clean, yet nontrivial. Despite the breakdown of axial symmetry we find stable orbits that are associated with adiabatic invariants and have simple geometrical representations. Resonant instabilities arise but can be avoided. A guiding-center approximation [6], a perturbation expansion using the method of multiple time scales [7], and exact numerical calculations are compared and discussed.

A charged particle (charge q and mass m) in a magnetic field, $B_0\hat{z}$, orbits in a right-handed circle about $\hat{z}$ at a positive cyclotron frequency $\omega_c = -qB_0/m$, with the right choice of direction for $\hat{z}$. This field and an electrostatic quadrupole (Fig. 2a) form a Penning trap. A charge at $\vec{r} = x\hat{x} + y\hat{y} + z\hat{z}$ acquires a potential energy,

$$W = m\omega_z^2[z^2 - (x^2 + y^2)/2]/2, \tag{1}$$

with a strength ω_z that will be identified as an angular frequency. The ratio $\epsilon \equiv \omega_z/\omega_c$ indicates the relative strength of the electric and magnetic binding. The trap is stable when $\epsilon < 1/\sqrt{2}$. Typically $\epsilon \ll 1$, as in the first simultaneous confinement of cold $\bar{p}$ (with $\epsilon = 1.5 \times 10^{-2}$) and e^+ (with $\epsilon = 2 \times 10^{-4}$) [8].

Adding the radial magnetic field of an Ioffe trap to $B_0\hat{z}$,

$$\vec{B} = B_0[\hat{z} + (x\hat{x} - y\hat{y})/R_0], \tag{2}$$

introduces a distance scale, R_0. Axial symmetry, present for large R_0, is destroyed as R_0 is reduced (e.g., by increasing the Ioffe current). Superconducting coils could produce an Ioffe gradient, $C_1 = B_0/R_0$, as large as 40 T/m, even for a bias field $B_0 = 2$ T, whereupon $R_0 = 5$ cm. A trapped particle is typically centered so that $r \ll R_0$.

An experimental realization (Fig. 1a) could direct the magnetic field of a solenoid (not pictured) along the axis of the stacked rings of an open-access Penning trap [9]. The Ioffe field would come from currents through vertical Ioffe bars and through "pinch coils" above and below. The

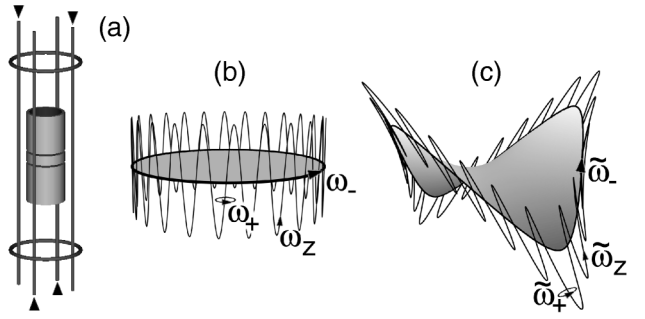

FIG. 1. (a) Open access Penning trap electrodes, with vertical current bars and pinch coils of an Ioffe trap. Orbits for a charged particle in a Penning trap (b) without and (c) with a radial Ioffe field.

 0031-9007/01/86(23)/5266(4)$15.00

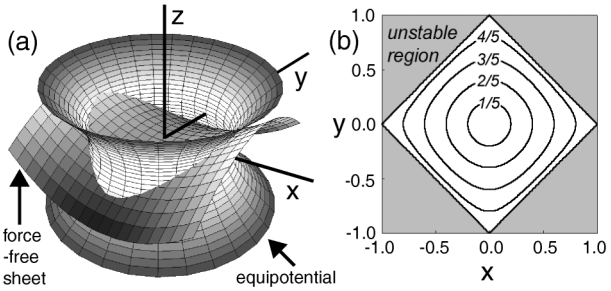

FIG. 2. (a) The force-free sheet and an equipotential of the electrostatic quadrupole. (b) Projections of stable magnetron orbits upon the xy plane lie within a square.

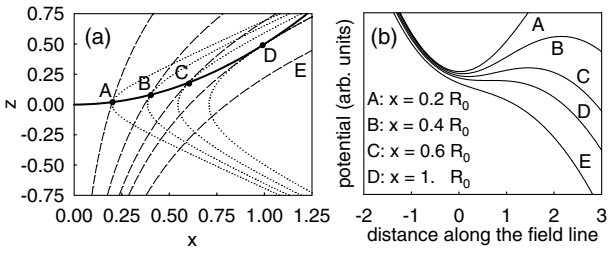

FIG. 3. (a) Magnetron orbits (dots) lie at the intersection of the force-free sheet (solid line) and equipotentials of the electrostatic quadrupole (dotted line), with magnetic field lines (dashed line). (b) The effective axial well depth decreases with increasing magnetron radius.

latter can be away from the central region where charged particles are trapped, so only the leading term of the radial magnetic field from Ioffe bars is in Eq. (2).

To simplify the equations of motion, from now on we scale times by $(\omega_c)^{-1}$ and distances by R_0, yielding

$$\ddot{x} = -\dot{y} + \epsilon^2 x/2 - y\dot{z}\,, \tag{3}$$

$$\ddot{y} = \dot{x} + \epsilon^2 y/2 - x\dot{z}\,, \tag{4}$$

$$\ddot{z} = -\epsilon^2 z + x\dot{y} + y\dot{x}\,. \tag{5}$$

The dynamics of a charge in a Penning-Ioffe trap (as in a Penning trap) are characterized by the single parameter ϵ; in useful traps $\epsilon \ll 1$. The nonlinear terms (e.g., $y\dot{z}$) are smaller than the linear terms so long as $r \ll 1$.

The nonlinear terms vanish near the center of the trap as well as when the Ioffe field is removed. The familiar solutions [1] then describe the three uncoupled oscillations of a charged particle in an ideal Penning trap.

$$u \equiv x + iy = ae^{i\omega_- t} + be^{i\omega_+ t}, \tag{6}$$

$$z = \mathrm{Re}(ce^{i\omega_z t})\,, \tag{7}$$

$$\omega_\pm = [1 \pm \sqrt{1 - 2\epsilon^2}\,]/2\,. \tag{8}$$

The oscillation frequencies are of different orders in the small parameter ϵ. The circular cyclotron oscillation is at high frequency $\omega_+ \approx 1$. The orthogonal harmonic axial oscillation is at intermediate frequency $\omega_z = \epsilon$, and the circular magnetron motion is at low frequency $\omega_- \approx \frac{1}{2}\epsilon^2$.

This frequency hierarchy is maintained in the Penning-Ioffe trap for small ϵ, the limit we consider first. Adiabatic invariants approximately preserve the exact Penning separation into three motions (Fig. 1c).

The fast cyclotron motion is perpendicular to the local magnetic field, rather than to $\hat{z}$, at the local cyclotron frequency $\tilde{\omega}_+ \approx \sqrt{1 + x^2 + y^2}$. This motion is much faster than any other and can be described by its magnetic moment, $M \approx mv_+^2/(2|\vec{B}|)$, located at a "guiding center" [6]. This moment is an adiabatic invariant [10]: as the local magnetic field changes, the cyclotron velocity v_+ (and radius) adjusts to keep M constant. Damping of the cyclotron motion (by synchrotron radiation for electrons, and by coupling to a tuned circuit for protons and ions) typically keeps it in thermal equilibrium with blackbody radiation or a cold resistor at some low temperature T. The resulting moment, with energy $MB \approx kT$, is typically much too small to noticeably affect the orbits.

The intermediate frequency "axial" oscillation is along the local magnetic field direction, as in the Penning trap. However, this direction is not $\hat{z}$, and the oscillation is not centered on the xy plane. Figure 3a shows magnetic field lines, $z = \ln(x/x_0)$, that cross the xy plane at x_0. The guiding center experiences an electric force parallel to its field line, $F_\parallel = -\vec{\nabla}W \cdot \hat{B}$. In the stable region of the trap, $F_\parallel$ is a restoring force that vanishes on

$$z = (x^2 - y^2)/2\,. \tag{9}$$

This force-free sheet (Fig. 2a) is the center of the axial oscillation; the guiding center damps to this surface when a resonant tuned circuit removes its axial energy. Figure 3b shows corresponding potential wells that are deeper nearer the center of the trap. Small oscillations in these are at the local axial oscillation frequency

$$\tilde{\omega}_z = \omega_z\sqrt{1 - x^2 - y^2}/\sqrt{1 + x^2 + y^2}\,. \tag{10}$$

The axial motion has an adiabatic invariant $J \approx E_z/\tilde{\omega}_z$. As the magnetron motion (discussed next) slowly changes a particle's radial position and hence its axial frequency, its axial energy E_z adjusts with $\tilde{\omega}_z$ to keep J constant.

The magnetron orbit is essentially the intersection of the force-free sheet and an equipotential of the electrostatic quadrupole potential (Fig. 2a). The guiding center is on the equipotential because the magnetron kinetic energy is much smaller than the potential energy, as in the Penning trap. Equations (3)–(5), with time scaled by ω_-^{-1}, can be integrated exactly for small ϵ to obtain an integral (easy to evaluate numerically) for the magnetron frequency,

$$\frac{1}{\tilde{\omega}_-} = \frac{8}{\pi\epsilon^2}\int_0^{\frac{\sqrt{2x_0^2 - x_0^4}}{2}} \frac{1 - 2v^2/\sqrt{1 - 2x_0^2 + x_0^4 + 4v^2}}{\sqrt{1 + v^2 - \sqrt{1 - 2x_0^2 + x_0^4 + 4v^2}}}\,dv\,, \tag{11}$$

for an orbit crossing the xz plane at $x = x_0$. Magnetron orbits near the center of the trap are circular with angular frequency ω_-. Larger orbits include odd harmonics of $\tilde{\omega}_-$ as they develop "corners"; symmetry under rotations about $\hat{z}$ by π suppresses even harmonics. The flux Φ enclosed by the magnetron orbit is an adiabatic invariant. For static magnetic fields, the invariance of Φ is equivalent to conservation of energy and adds nothing. If the Ioffe field strength was increased slowly (e.g., just before cold antihydrogen is formed), the magnetron radius and frequency would adjust to keep Φ constant.

The stable motions of a charge in a Penning-Ioffe trap pertain within an identifiable region. These orbits should be stable for exponentially long times [10] provided that resonances are avoided and adiabatic invariants are not otherwise broken. We discuss stability for small ϵ.

Projections of stable magnetron orbits on the xy plane lie within a square stability boundary (Fig. 2b) for small axial energy. Axial energy shrinks the boundary. Stable magnetron orbits of increasing radius (A–D in Fig. 3a) differ in effective axial well depth (Fig. 3b). This depth vanishes at D, the orbit whose projection is the square boundary. Beyond D there are no stable intersections between the force-free sheet and an energy equipotential.

Resonances $\tilde{\omega}_z = 2\tilde{\omega}_-$ must be avoided since these can cause the breakdown of the adiabatic invariants. The difficulty arises because the Ioffe field couples the axial and magnetron motions. A magnetron orbit takes the particle up and down in the z direction through two cycles (Fig. 1c), effectively "driving" the axial motion at angular frequency $2\tilde{\omega}_-$. If the axial frequency coincides with this "drive" frequency for a particular orbit, magnetron energy is transferred to the axial oscillation. Energy removed from the magnetron motion makes its radius grow until the particle eventually leaves the trap.

There are secondary resonances due to magnetron orbits away from the trap center having Fourier components at odd harmonics of $\tilde{\omega}_-$. These resonances are at $\tilde{\omega}_z = 2N\tilde{\omega}_-$, where $N > 1$ is an odd integer. We find that the frequencies for these shift out of resonance quickly enough with increasing radius to eliminate resonance and precipitous growth in the radial orbit size.

The resonances can be located using expansions around a Penning trap orbit [Eqs. (6) and (7)], utilizing the method of multiple time scales [7]. The expansions also reveal general features of the orbits, verify the guiding-center approximation, provide insight into the adiabatic invariants, and facilitate future experimental studies. We start from a Penning trap orbit with real a, and with b and c both real and small. We expand in powers of a, avoiding artificial divergences (sometimes called "secular resonances") by allowing the expansion amplitudes and phases to be relatively slowly varying functions of time.

We define $f(\omega) \equiv \omega^2 + \omega + \epsilon^2$, $g(\omega) \equiv \epsilon^2 - \omega^2$, and $h(\omega) \equiv 1 - 2\omega$ to display the Penning-Ioffe frequencies:

$$\tilde{\omega}_- = \omega_- + \frac{\omega_-^2}{g(2\omega_-)h(\omega_-)}a^2 + \frac{\omega_-^3}{g^2(2\omega_-)h(\omega_-)}\left[\frac{2}{h(\omega_-)} + \frac{\omega_-}{h^2(\omega_-)} - \frac{3\omega_-}{f(3\omega_-)} + \frac{8\omega_-^2}{g(2\omega_-)h(\omega_-)}\right]a^4 + \ldots, \tag{12}$$

$$\tilde{\omega}_z = \omega_z + \frac{\omega_z}{4}\left[\frac{1}{f(\omega_- - \omega_z)} + \frac{1}{f(\omega_- + \omega_z)}\right]a^2 + \frac{\omega_z}{2}\left[1 + \frac{7\epsilon^2}{2} + \ldots\right]a^4 - \frac{\omega_z}{4}\left[1 + \frac{15\epsilon^2}{4} + \ldots\right]a^4\cos 4\tilde{\omega}_- t + \ldots, \tag{13}$$

$$\tilde{\omega}_+ = \omega_+ + \frac{(\omega_+ + \omega_-)^2}{2g(\omega_+ + \omega_-)h(\omega_+)}a^2 - \frac{1}{8}[1 + 13\epsilon^2 + \ldots]a^4 + \frac{1}{8}\left[1 + \frac{7\epsilon^2}{2} + \ldots\right]a^4\cos 4\tilde{\omega}_m t + \ldots. \tag{14}$$

The exact a^4 coefficients for $\tilde{\omega}_z$ and $\tilde{\omega}_+$ are complicated enough that we display only the first terms in an expansion in ϵ. Frequency modulations arise from magnetron motion through the spatially varying magnetic field.

Figure 4a gives the magnetron orbit sizes at which the unwanted resonances $\tilde{\omega}_z = 2\tilde{\omega}_-$ occur for small cyclotron and axial energies. The series expansion (solid curve) is valid for orbits that are not too large. The guiding-center values (dashed curve) pertain for larger orbits and small ϵ. For a weak electrostatic field (i.e., small ϵ) the lowest order resonances are near the stability square in Fig. 2b. For a stronger electrostatic field (i.e., larger ϵ) the resonances occur for smaller orbits. The dots are example resonances identified using Fourier transforms of numerical solutions of the equation of motion. To the right of this resonance boundary, the adiabatic invariants which separate the axial and magnetron motion break down. We find no stable solutions in this region, except in the Penning trap limit of very small x. To the left of the resonance boundary, however, a charged particle in a Penning-Ioffe trap seems to be stable.

To check the stability, we use a Runge-Kutta algorithm to integrate the equations of motion [Eqs. (3)–(5)] for long times. In one example (Fig. 4a) we use $B_0 = 2$ T, $R_0 = 13$ cm, $\epsilon = 0.05$, and begin with a magnetron radius of

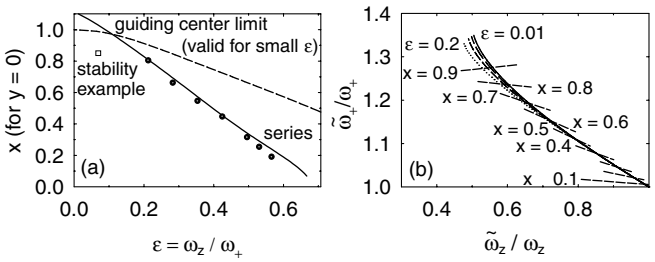

FIG. 4. (a) Magnetron orbit size that is troubled by resonance at $\tilde{\omega}_z = 2\omega_-$. Points are numerical confirmations. (b) Predicted relationship of the axial and the magnetron frequencies could be tested experimentally and used to determine the magnetron radius at $y = 0$.

0.85 and negligible axial and cyclotron energy. We detect no radial growth during 4×10^6 magnetron orbits; this is 31 s of real time.

The orbits are Fourier series in harmonics of the eigenfrequencies. For pure magnetron motion and small ϵ,

$$u_- = ae^{i\tilde{\omega}_- t} + \left[\frac{a^3}{8} + \frac{3a^5}{64}\right]e^{-3i\tilde{\omega}_- t} + \frac{a^5}{64}e^{5i\tilde{\omega}_- t}, \tag{15}$$

$$z_- = \left[\frac{a^2}{2} + \frac{a^4}{8} + \frac{3a^6}{64}\right]e^{2i\tilde{\omega}_- t} + \frac{3a^6}{128}e^{6i\tilde{\omega}_- t} \tag{16}$$

to $O(a^6)$. Substitution into Eqs. (1) and (9) explicitly confirms that this orbit lies on the electrostatic quadrupole and the force-free sheet. The exact coefficients of a^n for $\epsilon \neq 0$ are complicated functions of ϵ.

A small cyclotron oscillation adds

$$u_+ = be^{i\tilde{\omega}_+ t} - \frac{a^2 b}{4}e^{-i(\tilde{\omega}_+ + 2\tilde{\omega}_-)t} + \frac{a^4 b}{8}\left[e^{-i(\tilde{\omega}_+ + 2\tilde{\omega}_-)t} - \frac{1}{2}e^{-i(\tilde{\omega}_+ - 2\tilde{\omega}_-)t}\right], \tag{17}$$

$$z_+ = -abe^{i(\tilde{\omega}_+ + \tilde{\omega}_-)t} + \frac{a^3 b}{4}\left[e^{i(\tilde{\omega}_+ + \tilde{\omega}_-)t} - \frac{1}{2}e^{i(\tilde{\omega}_+ - 3\tilde{\omega}_-)t}\right], \tag{18}$$

$$b = b(t) = b(0)e^{-\frac{ia^4}{8}\cos 4\tilde{\omega}_- t}. \tag{19}$$

A small axial oscillation adds

$$u_z = \frac{ac}{2}[e^{-i(\tilde{\omega}_- - \tilde{\omega}_z)t} + e^{-i(\tilde{\omega}_- + \tilde{\omega}_z)t}] + \frac{a^3 c}{16}[e^{i(3\tilde{\omega}_- - \tilde{\omega}_z)t} + e^{i(3\tilde{\omega}_- + \tilde{\omega}_z)t}], \tag{20}$$

$$z_z = ce^{i\tilde{\omega}_z t}. \tag{21}$$

Substitution in the leading terms for M, J, and Φ also verifies that these are invariants through order a^4 for small ϵ. There is a delicate exact cancellation of the frequency and amplitude modulation terms.

Our predictions could be tested experimentally, starting with the predicted stability of a charge in a Penning-Ioffe trap. Second, the relationship of $\tilde{\omega}_z$ and $\tilde{\omega}_+$ could be compared with Eqs. (13) and (14) (Fig. 4b)—also a way to measure a. Third, the predicted resonant instability at $\tilde{\omega}_z = 2\tilde{\omega}_-$ could be confirmed as a function of a. Fourth, the frequency modulation spectra of $\tilde{\omega}_z$ and $\tilde{\omega}_+$ [Eqs. (13) and (14)] could be investigated.

In summary, a radial Ioffe field provides an experimentally realizable way to break the axial symmetry and a resulting confinement theorem for a Penning trap. Adiabatic invariants lead to the surprising prediction that a charged particle in a Penning-Ioffe trap is nonetheless stable for orbits within a stable volume, if resonances are avoided. The orbits have simple geometrical representations, expressions for the oscillation frequencies are given, and experimentally testable predictions are discussed.

Confining antiprotons and positrons in a nested version [11] of a Penning-Ioffe trap, along with cold antihydrogen atoms that are formed, now seems feasible for low particle densities. At a higher density, yet to be determined, collisions could break the adiabatic invariants, space charge could modify resonance frequencies, and collective plasma modes could be crucial. These effects may be more pronounced in a Malmberg-Ioffe trap [12] where oscillation frequencies are less well defined. The relationship of density and stability for charged plasmas in a Penning-Ioffe trap remains to be investigated.

We are grateful to R. Heller for initial conversations, and for NDSEG support to T. S. This work was supported by the ONR, the NSF, and the AFOSR.

[1] L. S. Brown and G. Gabrielse, Rev. Mod. Phys. **58**, 233 (1986).
[2] D. Dubin and T. O'Neil, Rev. Mod. Phys. **71**, 1 (1999).
[3] T. O'Neil, Phys. Fluids **23**, 2216 (1980).
[4] E. Backhaus, J. Fajans, and J. Wurtele, Phys. Plasmas **6**, 19 (1999).
[5] T. Bergeman, G. Erez, and H. Metcalf, Phys. Rev. A **35**, 1535 (1987).
[6] B. Lehnert, *Dynamics of Charged Particles* (Wiley, New York, 1964).
[7] C. Bender and S. Orszag, *Advanced Mathematical Methods for Scientists and Engineers* (McGraw-Hill, New York, 1978).
[8] G. Gabrielse, D. S. Hall, T. Roach, P. Yesley, A. Khabbaz, J. Estrada, C. Heimann, and H. Kalinowsky, Phys. Lett. B **455**, 311 (1999).
[9] G. Gabrielse, L. Haarsma, and S. Rolston, Int. J. Mass Spectrom. Ion Phys. **88**, 319 (1989); **93**, 121 (1989).
[10] T. Northrop, *The Adiabatic Motion of Charged Particles* (Wiley, New York, 1963).
[11] D. S. Hall and G. Gabrielse, Phys. Rev. Lett. **77**, 1962 (1996).
[12] E. Gibson and J. Fajans, in *Non-Neutral Plasma Physics III,* edited by John I. Bollinger, Ross L. Spencer, and Ronald C. Davidson, AIP Conf. Proc. No. 498 (AIP, Melville, NY, 1999), p. 250.